**Aalborg Universitet**

**AALBORG UNIVERSITY**
DENMARK

# Cost-Effective Prognostics of IGBT Bond Wires With Consideration of Temperature Swing

Hu, Keting; Liu, zhigang; Du, He; Ceccarelli, Lorenzo; Iannuzzo, Francesco; Blaabjerg, Frede; Tasiu, Ibrahim Adamu

IEEE POWER ELECTRONICS REGULAR PAPER/LETTER/CORRESPONDENCE

# Cost-Effective Prognostics of IGBT Bond Wires with Consideration of Temperature Swing

Keting Hu, *Student Member, IEEE*, Zhigang Liu, *Senior Member, IEEE*, He Du, *Student Member, IEEE*, Lorenzo Ceccarelli, *Student Member, IEEE*, Francesco Iannuzzo, *Senior Member, IEEE*, Frede Blaabjerg, *Fellow, IEEE*, and Ibrahim Adamu Tasiu, *Student Member, IEEE*

*Abstract-* **This paper presents a cost-effective prognostic method for the bond wires in IGBT. Consider that the crack propagation in the wire bond leads to the bond wire lift-off, the corresponding state equation is established from the fracture mechanics theory, with the consideration of the uneven distribution of the temperature swings. Hence, the proposed model can work under different loading conditions. With the fact that the on-state voltage ($v_{ce,on}$) of the IGBT shifts with the crack propagation, the history $v_{ce,on}$ is used to predict the remaining useful lifetime (RUL), through which numerous power cycling tests are avoided, and low economical cost for doing prognosis is fulfilled. In this paper, the functional relationship between the increase of $v_{ce,on}$ and the crack length of each bond wire is obtained through finite element simulation, while the effects of the temperature variation and metallization degradation to the $v_{ce,on}$ are compensated. Thus, the output equation can be obtained. Then, the unknown parameters of the above equations and the current crack length can be estimated by the particle-based marginalized resample-move algorithm. Finally, the RUL can be predicted effectively by evolving the particles obtained in the algorithm. The proposed method has been validated by the power cycling test.[1]**

**Index Terms—Bond wire lifetime, crack propagation, finite element, insulated gate bipolar transistor, marginalized resample-move.**

## I. INTRODUCTION

Insulated gate bipolar transistor (IGBT) based power converters are widely utilized in modern industry, including wind turbines [1], electrified vehicles [2-4], high current direct current electric power transmission systems [5, 6], etc. Though the power converter shows the great success in the industry, several papers have pointed out that the power converters take a significant part in the system failures, in which the power electronics component is one of the primary failure roots [7-9]. As a consequence, the reliability of power converters and especially the reliability of power electronics components have drawn considerable attention in recent years for the sake of safety and economy [10-13].

Package-related failure is one of the most common failures in IGBT modules, which is caused by the coefficients of thermal expansion (CTE) mismatch between different stacks inside the component [14]. When the IGBT is operating, periodical power losses are produced, and temperature swings are caused within the power module. Combined with the CTE mismatch, significant thermo-mechanical stresses are introduced to the joints between different stacks. Notably, the wire bonds and die-attach solder joints suffer higher stresses because of a more significant CTE mismatch. As a result, the bond wire degradation and solder fatigue are the two dominant wear-out failures in practice [15]. It should be pointed out that the former will be the focus of this paper, though both of them could degrade the performance of the IGBT module as time goes by, and destroy the component in the end, if no proper measures were taken.

Condition monitoring (CM) and prognostics are two fundamental approaches to improve the reliability of the IGBTs [12]. CM focuses on monitoring the damage sensitive parameters online to get an insight into the current health state of the IGBT. Once the unhealthy states or incipient faults have been detected, further actions will be implemented to avoid catastrophic consequences. On the other hand, the prognostics are capable of giving how much time the component can keep running functionally in the future, subjecting to specific loads. Consequently, the risk of failure could be minimized while the component is in service [16].

Usually, CM is the basis because it is impossible to perform the prognostics without any information about the component. The on-state voltage ($v_{ce,on}$) of the IGBT is the most chosen precursor, based on which numerous prognostic methods have been studied.

Generally, the prognostic methods can be classified into two categories, i.e., model-driven approach and data-driven approach. For the model-driven techniques, there are three main steps to predict the remaining useful lifetime (RUL) [17-20]. First of all, the mission profile of power converters should be translated into the junction temperature. With the help of the corresponding control strategy, wind speed, solar irradiance, or the driving speed will be converted to the input current and input voltage of operating converters. Then, the junction temperature of each IGBT can be obtained through the electro-thermal simulation or by the calculation of power

IEEE POWER ELECTRONICS REGULAR PAPER/LETTER/CORRESPONDENCE

loss and thermal impedance. Secondly, the temperature should be transferred to damage information on the component through an empirical lifetime model. The Coffin-Manson equation is a widely adopted model to describe the link between the junction temperature swing and the lifetime of IGBT. Later, the mean junction temperature, cycle frequency, power-on time, blocking voltage, current per bond wire, and the bond wire diameter are included in the lifetime model to get a more accurate characterization of the lifetime [21-24]. Finally, the accumulated damage of the corresponding mission profile can be computed based on the Miner's rule, and the RUL can be inferred as how many times the IGBT module could operate under this mission profile. However, it should be pointed out that with the degradation of the IGBT module, the junction temperature will rise under the same mission profile, because $v_{ce,on}$ increases and the heat dissipation path is reduced. Feedback from the damage accumulation to the electro-thermal simulation will be required to avoid over-optimistic results [17].

The data-driven methods mainly focus on the $v_{ce,on}$ data to extract the RUL information. Nevertheless, it is not easy to acquire enough data from the practical application in a short time, because the lifetime of the power module could be several years and even tens of years. To address this problem, the accelerated power cycling test could be a solution for validation [21, 25, 26]. By operating the power modules under high thermal stress, the components would degrade much faster than under normal operating conditions. Thus, the data collection can be finished within a few weeks and even several days. The most straightforward data-driven method is to predict the RUL by training. In [16], the $v_{ce,on}$ data are discretized into several phases depending on the IGBT health states. After the noise is filtered by a low-pass filter, the duration of each phase, together with the corresponding RUL are fed to a neural network (NN) and the adaptive neuro-fuzzy inference system (ANFIS) for training. The results show that NN outperforms ANFIS in the case of [16]. As an improved method, a stochastic process is combined with a time-delay neural network to predict the RUL, which can provide a confidence interval [27]. The uncertainty is also considered in [28]. It models the discrete degradation process by various probability distributions. Then, Monte Carlo simulations are carried out to estimate the precursor value up to the failure criterion. To enhance the prognostic ability for varying load conditions, the precursors could be unified before fed to the ANFIS [29].

Unfortunately, the performance of the aforementioned data-driven method is not so satisfying due to the small dataset scale. In spite of accelerated tests, it is still a problem to collect enough data in a short time. An alternative solution could be to utilize the history information. In [30], the available precursor data is collected to do curve fitting at some point of the lifetime, based on the knowledge of the failure process. Thus, the RUL can be fulfilled by extrapolating the precursor. The results indicate that the later the prediction is performed, the better the accuracy will be. A more sophisticated version of this method is to replace the

extrapolation with the particle filter (PF), which can deal with the uncertainty. In [31, 32], the sequential importance resampling PF and auxiliary PF (APF) are utilized to predict the RUL, respectively. It turns out that the APF has higher prediction accuracy and narrower probability density function. It should also be noted that the Mahalanobis distance between $v_{ce,on}$ and collector-emitter current ($I_{ce}$) is calculated to determine the anomaly and trigger the prediction in [31].

Though the above methods can achieve their successes in predicting the RUL, there are still challenges. For the model-driven approach, it requires numerous power cycling tests to find out the parameters of the empirical model, which is time-consuming and uneconomical. This problem could be more severe when more and more parameters are taken into the model. Meanwhile, the mission profile selection also requires further investigations. For the training methods of the data-driven approach, as mentioned earlier, the performance under small scale data should be improved. As for the history data-based methods, most of them hold the assumption that the load is constant, i.e., the temperature keeps steady throughout the whole lifetime. If the load is not constant, the fitted model may be different from the real one and leads to an unreliable result.

The contribution of this paper is given as below.
1) This paper proposes a fusion method of model-driven and data-driven approach, which inherits the advantages of both approaches to attain the cost-efficiency and the capability of dealing with temperature swing variation (TSV) condition at the same time.
2) The system model is established from the physics-of-failure view with the aid of finite element simulation, rather than by a simple curve fitting.
3) An accurate finite element model of the IGBT module is presented.
4) The features derived from the finite element analysis make it possible to describe the crack propagation processes of all the wire bonds simultaneously.
5) The temperature and metallization reconstruction effects on the $v_{ce,on}$ are compensated.

The rest of this paper is organized as follows. Section II contains the finite element simulation results. The system modeling with the temperature and metallization reconstruction consideration will be given in Section III. The lifetime prediction scheme is described in Section IV. Section
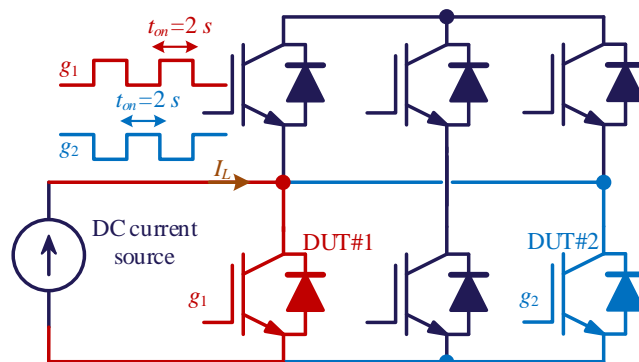


Fig. 1. Power cycling test configuration using a six-pack IGBT module.

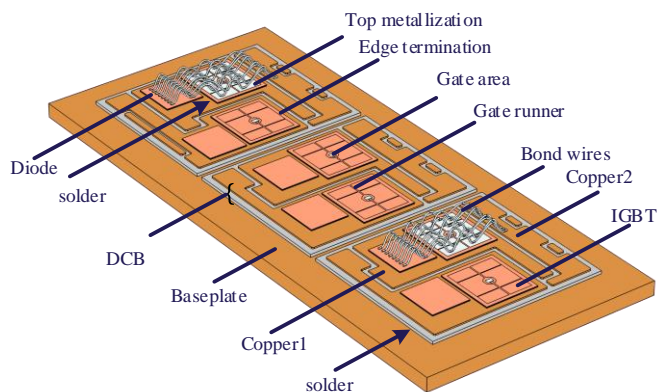IEEE POWER ELECTRONICS REGULAR PAPER/LETTER/CORRESPONDENCE
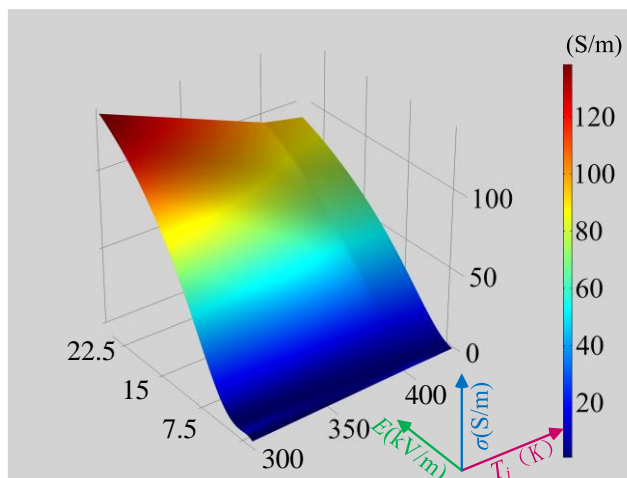


Fig. 2. Geometry of the finite element model of the six-pack IGBT module.



Fig. 3. Electrical conductivity of the die related to the temperature and electric field strength inside the die.

TABLE I
GEOMETRIC SIZE OF THE FINITE ELEMENT MODEL

| Layer | Material | Thickness (um) | Dimensions (mm×mm) |
|---|---|---|---|
| Bond wire | Aluminum | $\phi 375$ | none |
| Metallization | Aluminum | 3.2 | complied |
| IGBT | Silicon | 115 | 11.31×12.56 |
| Diode | Silicon | 115 | 8.15×9 |
| Die solder | SAC305 | 135 | complied |
| | Copper | 300 | 34.53×30.69 |
| DCB | $Al_2O_3$ | 600 | 37.125×33 |
| | Copper | 300 | 34.53×30.69 |
| Baseplate solder | SAC305 | 200 | complied |
| Baseplate | copper | 3000 | 50×115 |

TABLE II
THERMAL PROPERTIES OF THE MATERIALS [33, 34]

| Material | Property | Temperature (°C) | | |
|---|---|---|---|---|
| | | 25 | 125 | 225 |
| Aluminum | $k$ (W/m·K) | 237 | 240 | 236 |
| | $Cp$ (J/kg·K) | 897 | 955.5 | 994.8 |
| Silicon | $k$ (W/m·K) | 148 | 98.9 | 76.2 |
| | $Cp$ (J/kg·K) | 705 | 788.3 | 830.7 |
| SAC305 | $k$ (W/m·K) | 57 | 57 | 57 |
| | $Cp$ (J/kg·K) | 220 | 220 | 220 |
| Copper | $k$ (W/m·K) | 401 | 393 | 386 |
| | $Cp$ (J/kg·K) | 385 | 398.6 | 407.7 |
| $Al_2O_3$ | $k$ (W/m·K) | 37 | 27.2 | 20.9 |
| | $Cp$ (J/kg·K) | 785.5 | 942 | 1076 |

V presents the experimental results and Section VI gives the conclusion.

## II. FINITE ELEMENT SIMULATION

To establish the physics-of-failure model of the bond wire degradation process, the bond temperature is required to be known. Though the IR camera can measure the surface temperature of an open module, it is not applicable to measure the temperature of the bonds that are shielded by the bond wires. Besides, it is also not possible to link the temperature, bond crack length, and the increase of $v_{ce,on}$ together during the power cycling test. Given this circumstance, finite element simulations are carried out in COMSOL to tackle the above problems.

### A. Geometry

The configuration of the target power module can be seen in Fig. 1 and the geometrical model of the IGBT module is given in Fig. 2. To comply with the accelerated power cycling test condition, only the lateral IGBTs on the low side are stressed and analyzed in detail. The rest of IGBTs and all the diodes are simplified by removing the top metallization and bond wires without significant errors on the results. For each IGBT, the gate area is in the center of the IGBT, the gate runner

separates the active areas, and the termination is located at the edge. All of them do not carry the load current when the IGBT is conducting, which results in the uneven temperature distribution of the die. Besides, two solder layers are considered in the model. One is between the die and the DCB, while another lies between the DCB and the baseplate. TABLE I shows the geometry sizes of all the layers as mentioned above.

### B. Material Property and Boundary Condition

As it is well known that the material properties, i.e., thermal and electrical nature, are temperature-dependent, the temperature characterizations of the materials are taken into account in the finite element model. For the electrical parameters, the electrical conductivity governed by the temperature is considered. Linear approximation of the resistivity is adopted for the electrical conductivities of the aluminum and the copper, as shown in (1).

$$\frac{1}{\sigma(T)} = \frac{1}{\sigma_0}\left[1 + \beta(T - T_0)\right] \qquad (1)$$

where $\sigma$ represents the electrical conductivity at temperature $T$, $\sigma_0$ the electrical conductivity at the reference temperature, $\beta$ the temperature coefficient, and $T_0$ the reference temperature. According to [33], $\sigma_0 = 3.77 \times 10^7$ S/m and $\beta = 0.00404$ K$^{-1}$
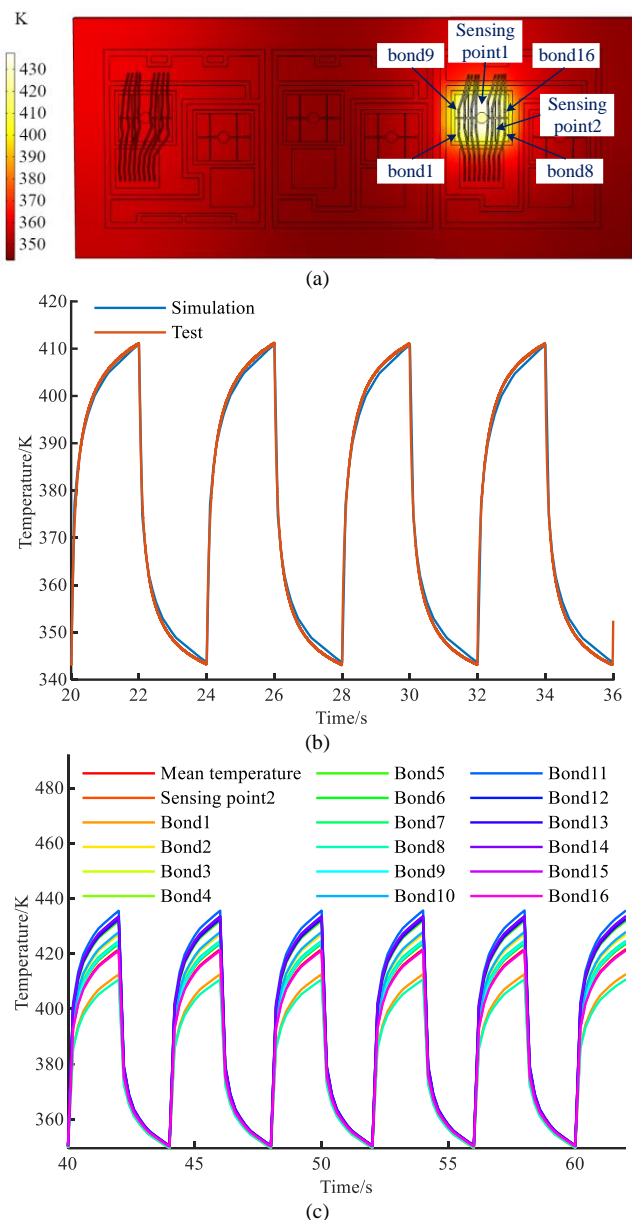
(a)



(b)



(c)

Fig. 4. Finite element simulation results (a) temperature distribution of the module when DUT#1 reaches the maximum temperature; (b) comparison between the simulation result and the test result; (c) simulation results of the temperatures of different parts inside the component.

for the aluminum and $\sigma_0 = 5.95 \times 10^7$ S/m and $\beta = 0.00390$ K$^{-1}$ for the copper, with the reference temperature at 20°C.

However, the electrical conductivity of the die active area will be realized in another way. Since the electrical conductivity not only depends on the temperature, but also the current flowing through it (or the voltage across it during conducting), the electrical conductivity at different current and temperature could be obtained through the datasheet. It should be pointed out that the curve tracer may not be applicable here because it measures the terminal-to-terminal voltage, instead of the voltage across the die. When applying the temperature- and current-/voltage- dependent $\sigma_{die}$ in the COMSOL, the main problem is that the current cannot be measured directly and the voltage is not distributed evenly inside the die. This

problem could be settled by introducing the electric field strength in the vertical axis, which is the quotient of voltage and distance. Thus, the interpolated $\sigma_{die}$ that is related to the temperature and electric field strength can be used in the finite element simulation, as shown in Fig. 3.

On the other hand, two thermal properties are included in the simulation, namely, the thermal conductivity ($k$) and the specific heat capacity ($Cp$), both of which depend on the temperature. Their values at different temperatures are as shown in TABLE II [33, 34].

The boundary conditions are set in line with the testing condition, i.e., the current source with 125A is set at Copper1 while Copper2 is set as the ground (see Fig. 2). Accordingly, the heat is generated in the dies and the bond wires at the same time, and alternately in DUT#1 and DUT#2. Meanwhile, the heat transfer coefficient is set to 875 W/m$^2$ K at the bottom of the baseplate to emulate the cooling plate and set to 50 W/m$^2$ K on the other surfaces to represent the natural cooling. The ambient temperature is set at 35 °C with the consideration that it will rise due to the heat dissipated by the module. Note that the boundary condition should be reset accordingly when the module operates in other applications.

*C. Simulation Results*

As mentioned above, only the maximum and minimum temperatures are recorded during the power cycling test, and a verification test is performed for the finite element simulation. It records the temperature continuously with a sampling frequency at 1 kHz when the module reaches the thermal equilibrium. Meanwhile, the simulated temperature is exported as well at the same sensing point (sensing point 1 in Fig. 4(a). Therefore, the uneven temperature distribution effects are negligible in this case. A comparison between the tests and the simulations is given in Fig. 4(b). It can be seen that the simulation matches well with the test, which shows the effectiveness of the finite element model.

Fig. 4 (a) depicts the simulated temperature distribution of the IGBT module. It can be concluded that the temperatures of different areas of the module are significantly different. The highest temperature point appears on the bond wire, and the temperature of the inner part of the active area is higher than the others. When comparing the temperatures of all the bonds, bond 11 is the hottest. The temperatures of different parts inside the component are given in Fig. 4(c), including all the bonds, the sensing point 2 and the average value of the active area of the die. The parameters mentioned above will be used to model the bond degradation process in Section III.

### III. STATE-SPACE MODEL OF THE DEGRADATION PROCESS

Primarily, the bond wire lift-off is caused by the thermo-mechanical stresses that initiate and propagate the cracks in the aluminum wire near the bond, from both edges. It is a typical fracture mechanics problem that has been studied since the last century. The process can be classified into three stages, namely, initiation, propagation and unstable region. Usually, the first stage consumes most of the lifetime to form the initial crack, with the help of cyclic stresses and the defects in the

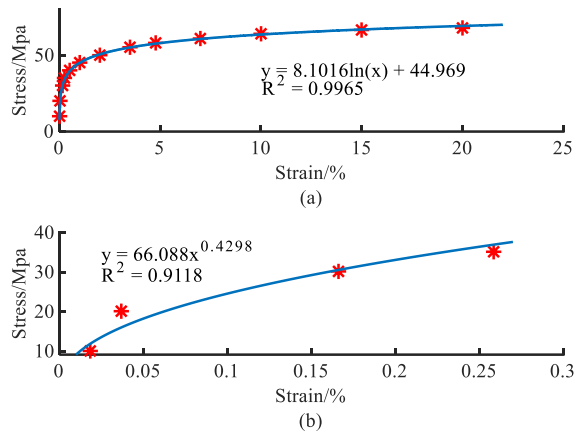IEEE POWER ELECTRONICS REGULAR PAPER/LETTER/CORRESPONDENCE



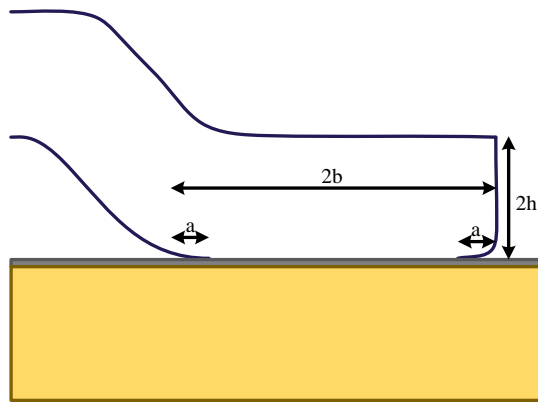Fig. 5. Stress-strain curve of the aluminum bond wire (a) for the whole range; (b) around working point [41].



Fig. 6. Instruction of the geometry parameters used.



Fig. 7. Number of cycles to failure of metallization as a function of $\Delta T$ [45].
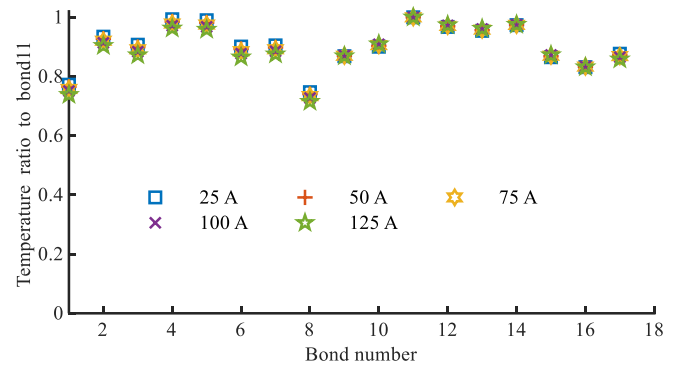


Fig. 8. Temperature ratio of each bond to bond 11 at different currents (bond 17 is the sensing point).

specimens. In the case of wire bonding, however, the situation may differ. According to [35-37], the ultrasonically wire bonding could damage the bonds and make them vulnerable, even pre-crack could have been the result. As a consequence, the lifetime of the bond wire could be regarded roughly as the time that propagating to the critical crack length needs. This assumption is the basis of the prognostic method in this paper.

*A. State Equation*

Consider the fact that the absolute junction temperature contributes much more to the solder fatigue than to the bond wire fatigue, the Paris' equation is selected here to describe the crack propagation as shown in equation (2) [38, 39].

$$\frac{da}{dN} = C(\Delta k)^m \tag{2}$$

where $a$ represents the crack length of one side for a double edge notch specimen, $N$ is the cycles, $\Delta k$ is the stress intensity factor, $C$ and $m$ are the constants.

Basically, $\Delta k$ is influenced by the cyclic stress $\Delta\sigma$, the geometry factor $Y$, and the crack length $a$, which can be described in (3).

$$\Delta k = \Delta\sigma \cdot Y \cdot \sqrt{\pi \cdot a} \tag{3}$$

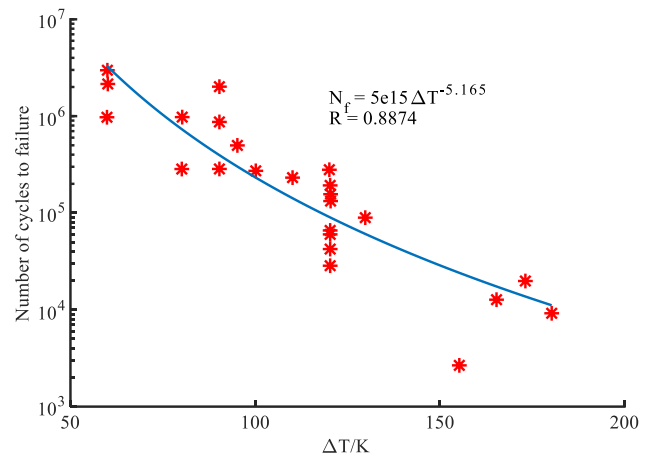$\Delta\sigma$ is caused by the combination of the temperature difference and the CTE mismatch, which can be obtained

through the stress-strain curve, as shown in Fig. 5(a) [40]. The strain is calculated as (4).

$$\Delta\varepsilon = \Delta\alpha \cdot \Delta T \tag{4}$$

Where $\Delta\alpha$ indicates the CTE difference between the aluminum and the silicon. Fig. 5(b) gives the stress-strain curve around the working point of the IGBT module, which will be used later to simulate the crack propagation.

The parameter $Y$ depends on the geometry information of the specimen. According to [41], it could be described as

$$Y = \sqrt{\pi \cdot a} \times$$

$$\frac{1.122 - 0.56\left(\frac{a}{b}\right) - 0.205\left(\frac{a}{b}\right)^2 + 0.471\left(\frac{a}{b}\right)^3 - 0.190\left(\frac{a}{b}\right)^4}{\sqrt{1 - \frac{a}{b}}} \tag{5}$$

where $b$ is half of the length of the specimen. Mohsin [42] pointed out, nevertheless, that the crack location information, i.e., the ratio between the crack length $a$, and the specimen height $2h$, as well as the ratio between the crack length and the specimen length, also influences $Y$, which will of course have an impact on the crack propagation rate. For the conciseness of the paper, the correctness factor is given directly here as 7.54, which is derived from the results in [42]. The parameters are given as $2h = 280\ \mu m$, $2b = 800\ \mu m$, and shown in Fig. 6.

Combining (2)-(5), the state equation of crack propagation can be described in (6).

IEEE POWER ELECTRONICS REGULAR PAPER/LETTER/CORRESPONDENCE

$$\frac{da}{dN} = C\left[\left(8.1016\times\left(\ln\left(\Delta\alpha\cdot\Delta T\times100\%\right)+44.969\right)\right)\cdot\sqrt{\pi\cdot a}\times7.54\times\right.$$
$$\left.\frac{1.122-0.56\left(\frac{a}{b}\right)-0.205\left(\frac{a}{b}\right)^2+0.471\left(\frac{a}{b}\right)^3-0.190\left(\frac{a}{b}\right)^4}{\sqrt{1-\frac{a}{b}}}\right]^{3.2}+\sigma_1 \quad (6)$$

where $\sigma_1$ is the process noise, and $m$ is given as 3.2 according to [43].

### B. Output Equation

The cracks in the bonds increase the resistance of the IGBT. As a consequence, $v_{ce,on}$ keeps rising during the aging, and it can be utilized as a precursor for the RUL. In reality, besides the bond wire degradation, $v_{ce,on}$ is affected by the other two factors, namely, temperature, and metallization degradation (solder fatigue can be regarded as temperature). Thus, it is important to consider these two when modeling the $v_{ce,on}$-based output equation.

### 1) Temperature

The value of $v_{ce,on}$ varies with the temperature significantly though the current keeps constant, as demonstrated in Fig. 3. As a result, the temperature component of $v_{ce,on}$ must be eliminated before the RUL prediction. Two mechanisms increase and decrease the voltage with the increasing temperature at the same time. When the current is low, $v_{ce,on}$ decreases with the temperature and the opposite for the high current. But for the same current, the temperature coefficient is almost constant for different temperatures and the temperature effects to $v_{ce,on}$ can be compensated as

$$v_{ce,on}^c = v_{ce,on} - \gamma\left(T - T_0\right) \quad (7)$$

where $v^c_{ce,on}$ represents the compensated $v_{ce,on}$, $\gamma$ is the temperature coefficient, $T$ indicates the corresponding temperature of the sampled $v_{ce,on}$, $T_0$ denotes the reference temperature.

### 2) Aluminum Metallization Reconstruction

The mismatching of CTE produces stress to the aluminum, which is large enough to cause plastic deformation and forms the hillocks and cracks in the metallization. As a result, the sheet resistance rises and $v_{ce,on}$ increases accordingly. The relationship between the number of cycles to failure and $\Delta T$ is given in Fig. 7, as obtained in [44]. The failure criterion is selected to be an 8% increase of $v_{ce,on}$. Thus, the voltage shift of each cycle can be approximated by (8).

$$\Delta v_{ce,on} = k\frac{8\%\times v_{ce,on0}}{5\times10^{15}\Delta T^{-5.165}} \quad (8)$$

where $v_{ce,on0}$ is the initial value of $v_{ce,on}$, and $k$ is a constant that to be identified. In fact, $k$ is a variable at the early stage and approaches to a constant later [45]. Therefore, if (8) is utilized in the evolution model of $v_{ce,on}$, it should wait until $k$ reaches a stable state. Generally, the data from another device could lead to a non-negligible error in the model. However, it could be acceptable here because the metallization is rather a general component without much difference between the different devices.

### 3) Bond Wire Lift-off

It was pointed out earlier that the voltage drop across the wire-bonds with respect to the bond crack can be expressed as (9) [30].
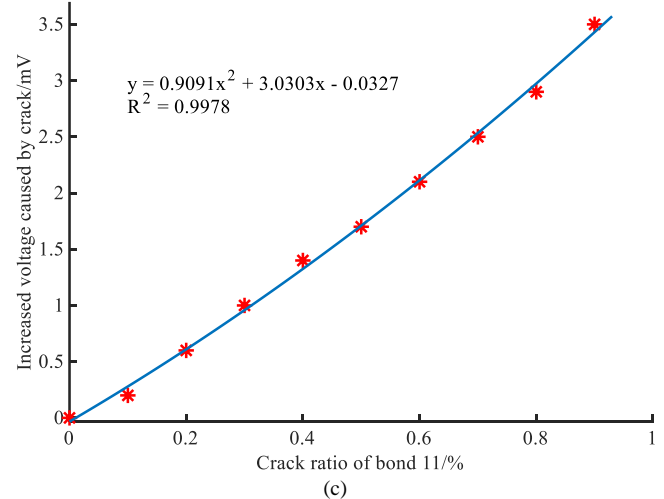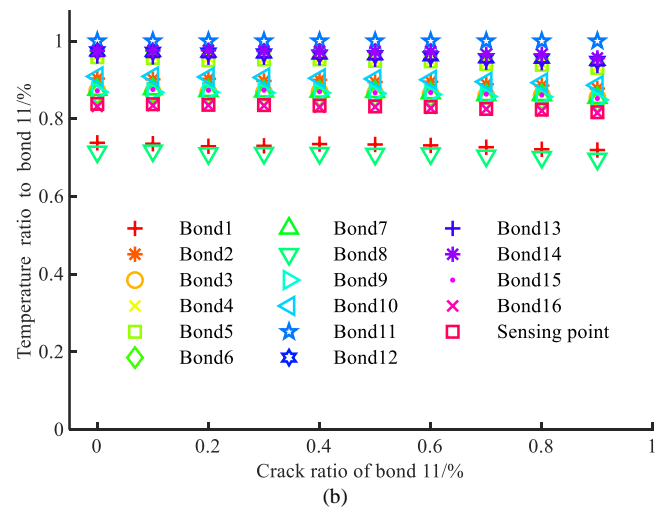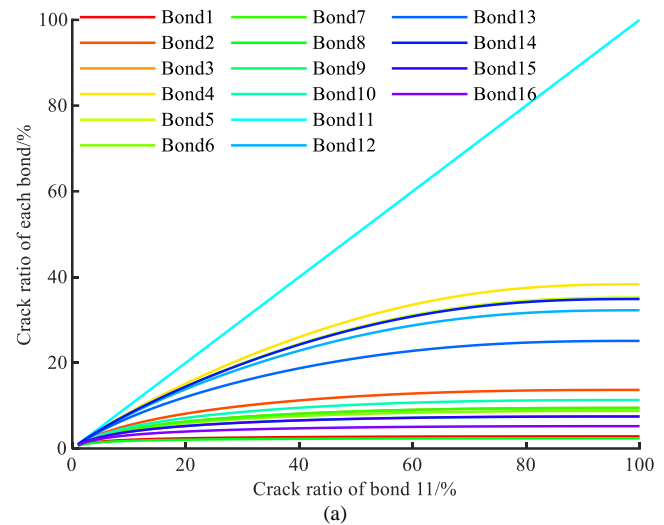


Fig. 9. (a) crack evolution with respect to bond 11 (b) temperature ratios of all the bonds to the bond 11 at different crack ratio of bond 11 (c) increased voltage caused by the crack with respect to the bond 11 crack length.

$$V_{WB} = v_0 + \frac{\eta}{1-\xi\cdot cycle} \quad (9)$$

where $V_{WB}$ is the wire-bonds voltage, $v_0$ is the initial voltage, $\eta$ and $\xi$ are the model parameters.

However, two problems should be noted for this equation. First, it implies that the crack propagation rate keeps constant all the time regardless of the crack length and the temperature, which is contradictory to (6). The reason for this may be that it is based on the results in [46], which is under high temperature that could trigger the recovery mechanism called annealing, and then, changes the crack propagation rate. Yet such a high temperature is unlikely to happen in practice. On the other hand, the initial voltage of the wire-bonds is difficult to know. Based on the above two reasons, a finite element simulation is preferred here to link the crack length and the increased voltage together, with consideration of the uneven temperature distribution.

Fig. 8 shows the finite element simulation results of the temperature ratio of each bond to the hottest bond 11 at different currents. It can be found that the ratios almost keep constant in spite of the load variation. This feature provides the possibility of simulating crack propagation under different loads. By substituting the stress-strain curve of Fig. 5(b) into (6), the crack propagation law can be obtained, as shown in (10).

$$\frac{da}{dN} = C\left[7.54 \times \left(66.088\left(\Delta\alpha \cdot \Delta T \times 100\%\right)^{0.4298}\right) \cdot \sqrt{\pi \cdot a} \times \right. \tag{10}$$

$$\left. \frac{1.122 - 0.56\left(a/b\right) - 0.205\left(a/b\right)^2 + 0.471\left(a/b\right)^3 - 0.190\left(a/b\right)^4}{\sqrt{1 - a/b}}\right]^{3.2} + \sigma_1$$

Then, the ratio of each bond crack length to the crack length of bond 11 is

$$\frac{\Delta a_i}{\Delta a_{11}} = \left(\left(\frac{\Delta T_i}{\Delta T_{11}}\right)^{0.4298} f(a_i, a_{11})\right)^{3.2} \tag{11}$$

where $\Delta a_i$ represents the crack increase of each bond, $\Delta a_{11}$ is crack increase of bond 11, $a_i$ is the crack length of each bond, and $a_{11}$ is the crack length of bond 11.

Thus, the crack propagation of each bond with respect to the crack length of bond 11 can be simulated as Fig. 9(a). The temperature ratios of all the bonds to the bond 11 at the different crack ratios of bond 11 is given in Fig. 9(b). It can be seen that the ratios are almost constant despite the crack length increasing, which demonstrates the effectiveness of the simulated crack length. Finally, the increased voltage with respect to the bond 11 crack length can be obtained through
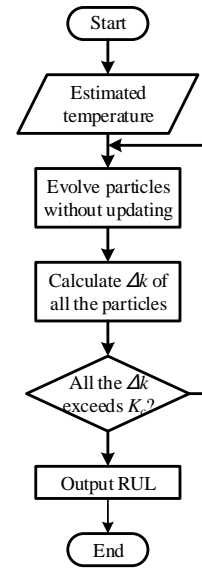


Fig. 10. Flowchart of the prediction method.

finite element simulation according to the crack propagation, as shown in Fig. 9(c).

Overall, the output equation, i.e., the evolution of $v_{ce,on}$ as a function of the crack ratio of bond 11, can be obtained as given in (12) in millivolts (temperature compensated).

$$v_{ce,on}^c = \underbrace{v_{ce,on0}}_{\text{initial value}} + \underbrace{0.9091\left(\frac{a_{11}}{b}\right)^2 + 3.0303\left(\frac{a_{11}}{b}\right) - 0.0327}_{\text{bond wire fatigue increase}} \tag{12}$$

$$+ \underbrace{\sum_{n=1}^{N} k \frac{8\% \times v_{ce,on0}}{5 \times 10^{15} \Delta T_{11n}^{-5.165}}}_{\text{reconstruction increase}} + \sigma_2$$

where $\Delta T_{11n}$ is the temperature swing of bond 11 at step $n$, $a_{11}$ can be calculated by (6), $\sigma_2$ represents the measurement noise.

So far, the state-space model of the degradation process has been established as given in (6) and (12).

### C. Failure Criterion

Though a 5% increase of $v_{ce,on}$ is widely adopted as the failure criterion of IGBTs in past works, another criterion is utilized in this paper. It is based on the knowledge that once the first bond wire is lifted off, the current densities of the rest wires become higher and accelerate the degradation process. This positive feedback grows more and more severe until the IGBT fails in a relatively short time. Thus, it is reasonable to
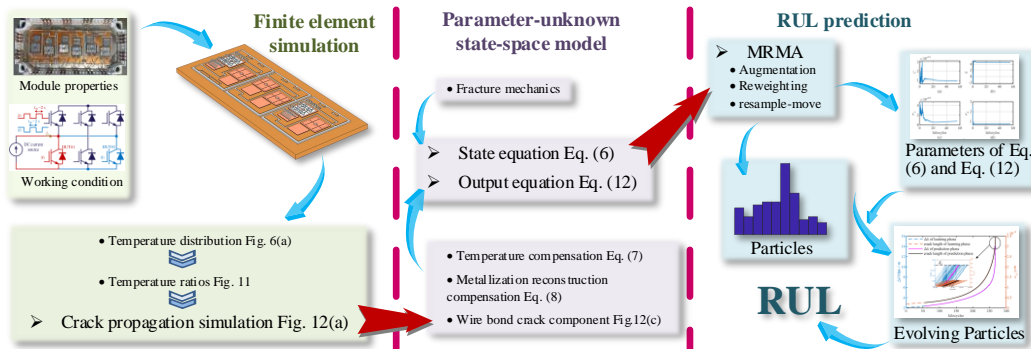


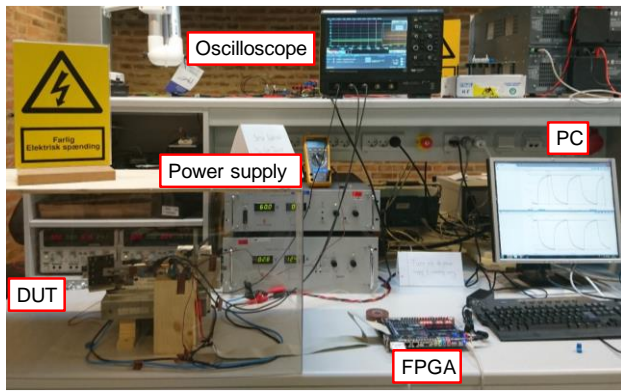Fig. 11. Schematic of proposed prognostic method.

IEEE POWER ELECTRONICS REGULAR PAPER/LETTER/CORRESPONDENCE



Fig. 12. Accelerated power cycling test set-up for six-pack IGBT module.



Fig. 13. Accelerated power cycling test results of the six-pack IGBT module.

select the first bond wire lift-off as the failure criterion. In this paper, once $\Delta k$ reaches the fracture toughness $K_c$ (14 MPa·m$^{1/2}$), which means the crack propagation enters the unstable region and the lift-off is considered to occur.

## IV. RUL PREDICTION

### A. Parameter Learning Algorithm

Though the state-space model of the crack propagation has been built in Section III, the model parameters $C$, $k$, $\sigma_1$ and $\sigma_2$ of (6) and (12) are still unknown. They must be identified before predicting the RUL. Here, MRMA is adopted for parameter learning and state estimation, which is proposed by Andras and Junye [47]. It can estimate the model parameter and the state sequentially when a new observation comes in, through the following three steps.

#### 1) Augmentation Step

Denote all the random quantities of the particle filter in step $l$ by $u_l$, the corresponding density is as given in (13) and the likelihood of the new observation is as written in (14).

$$\psi\left(u_{1:t}\middle|y_{1:t},\theta\right)=\prod_{l=2}^{t}\psi\left(u_l\middle|u_{l-1},y_l,\theta\right)\psi\left(u_1\middle|y_1,\theta\right) \quad (13)$$

$$\hat{p}\left(y_t\middle|y_{1:t-1},\theta\right)\equiv\hat{p}\left(y_t\middle|u_t,u_{t-1},\theta\right) \quad (14)$$

where $y$ represents the observation and $\theta$ is the parameter set.

Samples drawn from $\psi(u_t|u^{(n)}_{t-1}, y_t, \theta^{(n)})$ can be obtained by running the particle filter on the new observation $y_t$ for each $\theta$, which can reduce the computation burden.

#### 2) Reweighting Step

The incremental weights are calculated by using the equation (14). Thus, the updated weights can be given in (15).

$$s_t^{(n)}=s_{t-1}^{(n)}\times\hat{p}\left(y_t\middle|u_t^{(n)},u_{t-1}^{(n)},\theta^{(n)}\right) \quad (15)$$

Meanwhile, the likelihood of the parameters is given as

$$\hat{p}\left(y_{1:t}\middle|\theta\right)^{(n)}=\hat{p}\left(y_{1:t-1}\middle|\theta\right)^{(n)}\times\hat{p}\left(y_t\middle|u_t^{(n)},u_{t-1}^{(n)},\theta^{(n)}\right) \quad (16)$$

Then, the target distribution can be approximated by the weighted sample $\{(\theta^{(n)},u_t^{(n)},\hat{p}(y_{1:t}|\theta)^{(n)}),s_t^{(n)}\}$.

#### 3) Resample-Move Step

To maintain the effective particle size, the resample process will be executed once the effective particle size falls below the threshold $B_1$. Afterward, if the unique particles fall below the threshold $B_2$, each particle will be moved through a Markov kernel to enhance the diversity of the particles, without
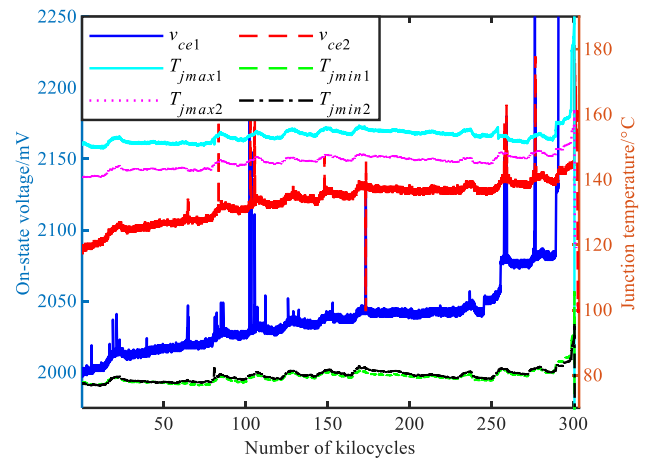
changing the original distribution. Please refer to [48] for more details of the algorithm.

### B. State Estimation and RUL prediction

After the parameters have been identified, the state of the crack length of bond 11 at step $t$ can be estimated by

$$a_{11,t}=\sum_{n=1}^{100}x_t^{(n)}\cdot w_t^{(n)} \quad (17)$$

where $x^{(n)}$ are the particles for the state and $w^{(n)}$ are the corresponding normalized weights, both are at step $t$.

The prediction method is similar to the conventional history-data-based approach. The particles produced by MRMA, which can approximate the posterior distribution of the crack length of bond 11 will evolve step by step according to (10) until all of them reach the failure criteria. Note the predictions will not be corrected by the future $v_{ce,on}$ which is unavailable at the prediction step. Then, substituting (4), (5), and (17) into (3), $\Delta k$ at step $t$ can be obtained. Consequently, the ending step that the $\Delta k$ exceeds the $K_c$ can be predicted and the RUL can be estimated. The flowchart of the prediction method is given in Fig. 10. Though the future junction temperatures are also unavailable, it could be estimated by the history mission profile for the repetitive load applications. Thus, the following prediction results of DUT#1 are based on the fact that the future temperature is known. The overall schematic of the prognostics is given in Fig. 11.

## V. EXPERIMENTAL RESULTS AND COMPARISONS

### A. Power Cycling Test

To collect the history data of $v_{ce,on}$, and validate the proposed prognostic method, the accelerated power cycling test has been performed on a commercial IGBT module (FS150R12KT4 from Infineon). It is a six-pack trench field stop module capable of blocking 1200 V voltage and conducting 150 A current. The configuration of the test set-up is shown in Fig. 1. The DC current source is utilized to provide the 125 A current to the two components under test (DUTs). The DUTs are triggered by an FPGA alternately for 2 seconds with +15/-10 V gate voltage, through which they will
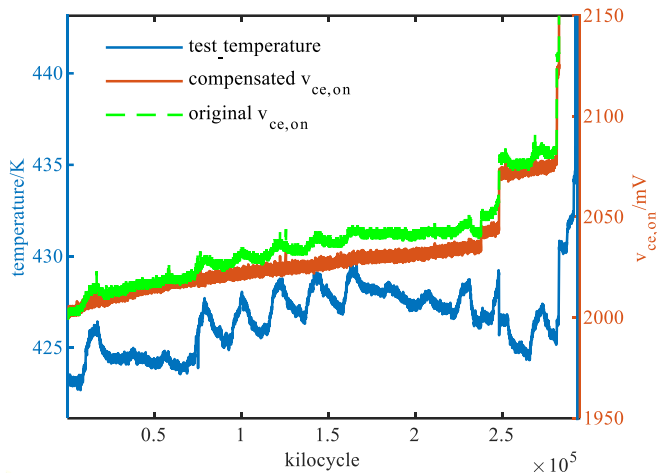
IEEE POWER ELECTRONICS REGULAR PAPER/LETTER/CORRESPONDENCE



Fig. 14.   Temperature compensation of DUT#1 $v_{ce,on}$.
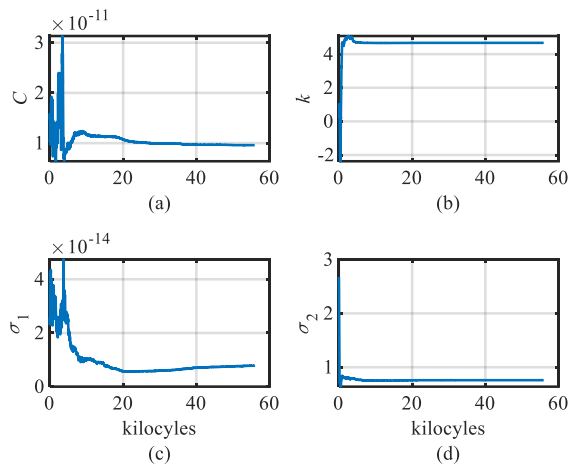


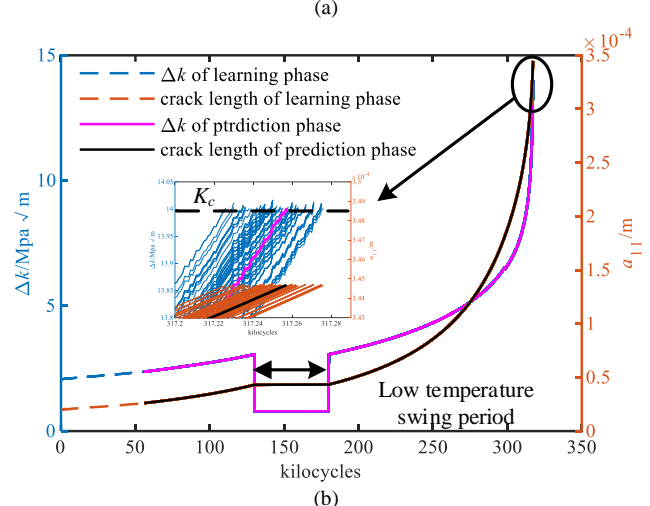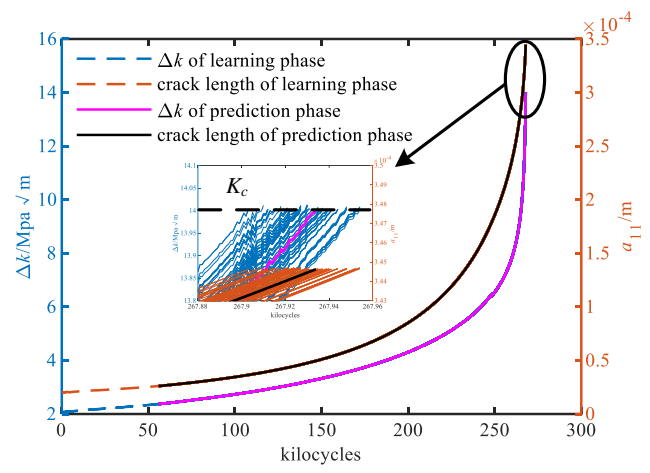Fig. 15.   State-space model parameters learned by MRMA.



Fig. 16.   Prediction results when (a) future temperature can be estimated. (b) future temperature can be estimated and includes low-temperature swing.

be heated by the power loss and cooled by the cooling plate repeatedly. As a consequence, sizeable thermo-mechanical stress is applied to the DUTs, and the aging process is accelerated.

The overall system is depicted in Fig. 12. During the power cycling test, the maximum junction temperature, minimum junction temperature and $v_{ce,on}$ are recorded for each cycle. The junction temperature is approximated by the die surface temperature, which is measured by putting an optical filter on the die surface. As for $v_{ce,on}$, it is measured by voltage probes of the oscilloscope. The test lasts for about 300 kilocycles until the gate-emitter short of DUT#1 (see Fig. 1) occurs. This could be attributed to the bond wire lift-off, which leads to the large current in remaining bond wires and forms a local hotspot around the left wire bonds on the chip [33].

The results are given in Fig. 13. The $v_{ce1}$, $T_{jmax1}$ and $T_{jmin1}$ represent the on-state voltage, maximum junction temperature and minimum junction temperature of DUT#1, while $v_{ce2}$, $T_{jmax2}$ and $T_{jmin2}$ indicate the same parameters for the DUT#2. The initial $T_j$ of DUT#1 is from 77.3°C to 150.2°C, with 72.9°C temperature variation ($\Delta T$). On the other hand, $\Delta T$ of DUT#2 is 63.4 °C, which varies from 77.2°C to 140.6°C. It explains the fact that DUT#2 is still in good health state (no $v_{ce,on}$ jump is found in DUT#2) when DUT#1 has failed, as it

suffers lower thermo-mechanical stress. All of the temperatures rise during the power cycling test due to the increase of both $v_{ce,on}$ and thermal resistance of DUT caused by degradation. The fluctuation of the temperature could be caused by daylight during the sunny days.

*B. Temperature Compensation Results*

By taking the first sampled maximum temperature as the reference, the compensated results of DUT#1 $v_{ce,on}$ evolution is shown in Fig. 14. It can be seen that both the temperature fluctuations caused by the daylight and the temperature drift caused by the increasing power loss can be compensated adequately. It should be noted that the initial phase, when $v_{ce,on}$ increases while the temperature goes down, has been disregarded. This phenomenon could be attributed to the adjustment of the TIM. Meanwhile, the measurement spikes are filtered out for better prediction performance.

*C. Parameter Learning Results*

The initial guess of the unidentified parameters is given as

$$\theta_0 = \{C_0, k_0, \sigma_1, \sigma_2\} = \{5 \times 10^{-12}, 1, 5 \times 10^{-14}, 3\} \qquad (18)$$

The particle size is set as $100 \times 100$ for the parameters and state. The thresholds of $B_1$ and $B_2$ are 50 and 50, respectively.

The learning phase stops when all the parameters approach the stable state. In the case of DUT#1, it is about 56k cycles, and the estimated values of the parameters are as shown in Fig. 15, which are $\{9.59 \times 10^{-12}, 4.67, 7.80 \times 10^{-15}, 0.76\}$.

### C. RUL prediction results

The temperature measured during the power cycling test is used directly to represent the estimation of the temperature. The results are shown in Fig. 16(a). The IGBT is predicted to fail at 268k cycle when the $\Delta k$ exceeds the $K_c$, while the actual failure time is 238k cycle, indicating the prediction error is 12.61%. To validate the effectiveness of the temperature swing sensitivity, a period of 50k cycles with $\Delta T=5°C$ is inserted at 130k cycle. Given the fact that the IGBT degrades so slow under such small $\Delta T$, the actual lifetime is considered as 288k cycles. The prediction results are shown in Fig. 16(b), which is 317k cycles, with the prediction error of 10.07%. It could also be seen from the plateaus of both the crack length and $\Delta k$ that the extrapolation methods are not applicable in this case, neither from the curve-fitting perspective nor the fracture mechanics approach.

### D. Comparison with Conventional Methods
#### 1) Comparison with model-driven methods

To show the cost-effectiveness, the comparison between the proposed method and the conventional data-driven methods is given in Table III in terms of the minimum number of required power cycling tests $N_{pc}$. It can be seen that the conventional methods require 2-7 $N_{pc}$ while the proposed method requires no power cycling tests for parameter tuning (the power cycling test presented in this section is for validation). It should be pointed out that $N_{pc}$ is the minimum number that ensures the parameters can be calculated. More tests will be required if an accurate lifetime model is desired. In this sense, the proposed method is more cost-effective than conventional model-driven methods.

#### 2) Comparison with data-driven methods

To show the capability of dealing with varied temperature swings, the comparison between the proposed method and the curve fitting/filter-based data-driven methods is given in Table IV. It must be pointed out that the curve fitting/filter-based data-driven methods are based on $v_{ce,on}$ and the failure criterion is 5% increase of $v_{ce,on}$, which results in the lifetime equaling 280k cycles without TSV and 330k cycles with TSV. The curve-fitting equation is based on (9) and the fitted equation is given in (19). Its prediction results with and without temperature swing variation are both 338k cycles because it is not able to use the temperature information. As a result, the prediction errors ($e_p$) are 20.71% and 2.42% for the different conditions. Note that it is just a coincidence that $e_p$ of the condition with TSV is so low. If the duration of the low-temperature swing is set as 150k cycles, the prediction error would be large (-21.4%).

$$v_{ce,on} = 2002 + 0.00029 \times cycle + \frac{0.1654}{1 - 0.6652 \times cycle} \tag{19}$$

**Table III**
**COMPARISON OF $N_{pc}$**

| Methods | C-M$^*$ | A-C-M$^*$ | Method in [23] | Proposed method |
|---|---|---|---|---|
| $N_{pc}$ | 2 | 3 | 7 | 0 |

*C-M: Coffin-Manson model; A-C-M: Arrhenius-Coffin-Manson model

**Table IV**
**COMPARISON OF PREDICTION ERROR**

| Condition | Prediction error/$e_p$ | | | |
|---|---|---|---|---|
| | Curve fitting | PF | APF | Proposed method |
| w/o TSV | 20.71% | -10.14% | -9.29% | 12.61% |
| w/ TSV | 2.42% | -23.76% | -23.03 | 10.07% |
| $\Delta e_p^*$ | 18.29% | 13.62% | 13.74% | 2.54% |

*: $\Delta e_p$ = difference of prediction errors w/ and w/o TSV

The equation used for PF and APF are the same as [31], and the fitted model is given in (20).

$$v_{ce,on,n} = v_{ce,on,n-1} + 2 \times 2.164 \times 10^{-12} \times cycle + 0.000396 \tag{20}$$

The prediction results of PF and APF for both conditions are 251.6k cycle and 254k cycles.

It can be seen from Table IV that the prediction errors of all the three conventional methods are of huge difference under different conditions while the proposed method has a robust performance, which shows its advantage of dealing with TSV condition.

### VI. CONCLUSION

A cost-effective prognostic method for IGBT bond wire that considers the temperature swing has been presented in this paper. The conclusions can be drawn as follows.

(1) $v_{ce,on}$ could be a good indicator for predicting the RUL. Nevertheless, the irrelevant component, e.g., the voltage shift caused by the temperature variation or other degradation mechanisms, must be compensated before prediction.

(2) The relationship between the increase of $v_{ce,on}$ and the degradation state of the bond wire can be revealed by the finite element simulation.

(3) The temperature ratio of each bond to the hottest bond is almost kept constant under different load currents and degradation states.

(4) The system model is established from the fracture mechanism theory. Compared to the conventional model-based methods, it does not require a large number of power cycling tests, which can reduce the temporal and economic costs.

(5) The particle-based MRMA can estimate the unknown parameters of the system model.

(6) The proposed method can predict the RUL under temperature swing variation if the temperature information can be obtained, with a prediction error of about 10%. The error could be introduced from 1) the curve fittings; 2) temperature compensation or system modeling; 3) parameter learning algorithm; 4) disregard of the initial phase.

It should be pointed out that the temperature is measured by the optical fibers, which are unlikely to be used in practice. In this case, temperature-sensitive electrical parameters that are not affected by degradation could be a solution.

IEEE POWER ELECTRONICS REGULAR PAPER/LETTER/CORRESPONDENCE

## References

[1] V. Yaramasu, B. Wu, P. C. Sen, S. Kouro, and M. Narimani, "High-power wind energy conversion systems: State-of-the-art and emerging technologies," *Proceedings of the IEEE,* vol. 103, no. 5, pp. 740-788, 2015.

[2] L. Dorn-Gomba, P. Magne, B. Danen, and A. Emadi, "On the Concept of the Multi-Source Inverter for Hybrid Electric Vehicle Powertrains," *IEEE Transactions on Power Electronics,* vol. 33, no. 9, pp. 7376-7386, 2018.

[3] T. Kim and S. Kwak, "A Flexible Voltage Bus Converter for the 48-/12-V Dual Supply System in Electrified Vehicles," *IEEE Transactions on Vehicular Technology,* vol. 66, no. 3, pp. 2010-2018, 2017.

[4] H. Chen, H. Kim, R. Erickson, and D. Maksimovic, "Electrified Automotive Powertrain Architecture Using Composite DC-DC Converters," *IEEE Transactions on Power Electronics,* vol. 32, no. 1, pp. 98-116, 2017.

[5] D. L. H. Aik and G. Andersson, "Fundamental Analysis of Voltage and Power Stability of Single-Infeed Voltage-Source Converter HVDC Systems," *IEEE Transactions on Power Delivery,* vol. 34, no. 1, pp. 365-375, 2019.

[6] S. P. Engel, M. Stieneker, N. Soltau, S. Rabiee, H. Stagge, and R. W. D. Doncker, "Comparison of the Modular Multilevel DC Converter and the Dual-Active Bridge Converter for Power Conversion in HVDC and MVDC Grids," *IEEE Transactions on Power Electronics,* vol. 30, no. 1, pp. 124-137, 2015.

[7] B. Gou, "Fault diagnosis and fault-tolerant control technology of railway electrical traction converter," Ph.D. dissertation, Department of electrical engineering, Southwest Jiaotong University, Chengdu, China, 2016.

[8] L. M. Moore and H. N. Post, "Five years of operating experience at a large, utility-scale photovoltaic generating plant," *Progress in Photovoltaics: Research and Applications,* vol. 16, no. 3, pp. 249-259, 2008.

[9] S. Yang, A. Bryant, P. Mawby, D. Xiang, L. Ran, and P. Tavner, "An Industry-Based Survey of Reliability in Power Electronic Converters," *IEEE Transactions on Industry Applications,* 1 vol. 47, no. 3, pp. 1441-1451, 2011.

[10] H. Wang, M. Liserre, F. Blaabjerg, P. D. P. Rimmen, J. B. Jacobsen, T. Kvisgaard, and J. Landkildehus, "Transitioning to Physics-of-Failure as a Reliability Driver in Power Electronics," *IEEE Journal of Emerging and Selected Topics in Power Electronics,* vol. 2, no. 1, pp. 97-114, 2014.

[11] H. Wang, M. Liserre, and F. Blaabjerg, "Toward Reliable Power Electronics: Challenges, Design Tools, and Opportunities," *IEEE Industrial Electronics Magazine,* vol. 7, no. 2, pp. 17-26, 2013.

[12] H. Oh, B. Han, P. McCluskey, C. Han, and B. D. Youn, "Physics-of-Failure, Condition Monitoring, and Prognostics of Insulated Gate Bipolar Transistor Modules: A Review," *IEEE Transactions on Power Electronics,* vol. 30, no. 5, pp. 2413-2426, 2015.

[13] C. Busca, R. Teodorescu, F. Blaabjerg, S.Munk-Nielsen, L. Helle, T. Abeyasekera, and P. Rodriguez, "An overview of the reliability prediction related aspects of high power IGBTs in wind power applications," *Microelectronics Reliability,* vol. 51, no. 9-11, pp. 1903-1907, 2011.

[14] X. Fang, S. Lin, X. Huang, F. Lin, Z. Yang, and S. Igarashi, "A review of data-driven prognostic for IGBT remaining useful life," *Chinese Journal of Electrical Engineering,* vol. 4, no. 3, pp. 73-79, 2018.

[15] U.-M. Choi and F. Blaabjerg, "Separation of Wear-Out Failure Modes of IGBT Modules in Grid-Connected Inverter Systems," *IEEE Transactions on Power Electronics,* vol. 33, no. 7, pp. 6217-6223, 2018.

[16] M. Ahsan, S. Stoyanov, and C. Bailey, "Data driven prognostics for predicting remaining useful life of IGBT," in Proceedings of 39th International Spring Seminar on Electronics Technology (ISSE), Pilsen, Czech Republic, 18-22 May, 2016, pp. 273-278.

[17] H. Huang and P. A. Mawby, "A Lifetime Estimation Technique for Voltage Source Inverters," *IEEE Transactions on Power Electronics,* vol. 28, no. 8, pp. 4113-4119, 2013.

[18] P. Diaz Reigosa, H. Wang, Y. Yang, and F. Blaabjerg, "Prediction of Bond Wire Fatigue of IGBTs in a PV Inverter under a Long-Term Operation," *IEEE Transactions on Power Electronics,* vol. 31, no. 10, pp. 7171-7182, 2015.

[19] L. R. GopiReddy, L. M. Tolbert, B. Ozpineci, and J. O. P. Pinto, "Rainflow Algorithm-Based Lifetime Estimation of Power Semiconductors in Utility Applications," *IEEE Transactions on Industry Applications,* vol. 51, no. 4, pp. 3368-3375, 2015.

[20] M. Musallam, C. Yin, C. Bailey, and M. Johnson, "Mission Profile-Based Reliability Design and Real-Time Life Consumption Estimation in Power Electronics," *IEEE Transactions on Power Electronics,* vol. 30, no. 5, pp. 2601-2613, 2015.

[21] M. Held, P. Jacob, G. Nicoletti, P. Scacco, and M.-H. Poech, "Fast Power Cycling Test for IGBT Modules in Traction Application," in Proceedings of 2nd International Conference on Power Electronics and Drive Systems (PEDS), Singapore, 26-29 May, 1997, pp. 425-430.

[22] A. Syed, "Limitations of Norris-Landzberg equation and application of damage accumulation based methodology for estimating acceleration factors for Pb free solders," in Proceedings of 11th International Thermal, Mechanical & Multi-Physics Simulation, and Experiments in Microelectronics and Microsystems (EuroSimE), Bordeaux, France, 26-28 April, 2010, pp. 1-11.

[23] R. Bayerer, T. Herrmann, T. Licht, J. Lutz, and M. Feller, "Model for Power Cycling lifetime of IGBT Modules – various factors influencing lifetime," in Proceedings of 5th International Conference on Integration of Power Electronics Systems (CIPS), Nuremberg, Germany, 18-22 March, 2008, pp. 1-6.

[24] N. Dornic, Z. Khatir, S-H. Tran, A. Ibrahim, R. Lallemand, J.P. Ousten, J. Ewanchuk, and S. Mollov, "Stress-based Model for Lifetime Estimation of Bond-Wire Contacts using Power Cycling Tests and Finite Element Modelling," *IEEE Journal of Emerging and Selected Topics in Power Electronics,* to be published. DOI: 10.1109/JESTPE.2019.2918941.

[25] H. Berg and E. Wolfgang, "Advanced IGBT modules for railway traction applications- Reliability testing," *Microelectronics Reliability,* vol. 38, pp. 1319-1323, 1998.

[26] V. Smet, F. Forest, J.-J. Huselstein, F. Richardeau, Z. Khatir, S. Lefebvre, and M. Berkani, "Ageing and Failure Modes of IGBT Modules in High-Temperature Power Cycling," *IEEE Transactions on Industrial Electronics,* vol. 58, no. 10, pp. 4931-4941, 2011.

[27] A. Alghassi, S. Perinpanayagam, and M. Samie, "Stochastic RUL Calculation Enhanced With TDNN-Based IGBT Failure Modeling," *IEEE Transactions on Reliability,* vol. 65, no. 2, pp. 558-573, 2016.

[28] A. Alghassi, S. Perinpanayagam, M. Samie, and T. Sreenuch, "Computationally Efficient, Real-Time, and Embeddable Prognostic Techniques for Power Electronics," *IEEE Transactions on Power Electronics,* vol. 30, no. 5, pp. 2623-2634, 2015.

[29] M. Samie, A. Alghassi, and S. Perinpanayagam, "Unified IGBT prognostic using natural computation," in Proceedings of 2015 IEEE International Conference on Digital Signal Processing (DSP), Singapore, 21-24 July, 2015, pp. 698-702.

[30] N. Degrenne and S. Mollov, "Experimentally-Validated Models of On-State Voltage for Remaining Useful Life Estimation and Design for Reliability of Power Modules," in Proceedings of 10th International Conference on Integrated Power Electronics Systems, Stuttgart (CIPS), Germany, 20-22 March, 2018, pp. 1-6.

[31] N. Patil, D. Das, and M. Pecht, "A prognostic approach for non-punch through and field stop IGBTs," *Microelectronics Reliability,* vol. 52, no. 3, pp. 482-488, 2012.

[32] M. S. Haque, S. Choi, and J. Baek, "Auxiliary Particle Filtering-Based Estimation of Remaining Useful Life of IGBT," *IEEE Transactions on Industrial Electronics,* vol. 65, no. 3, pp. 2693-2703, 2018.

[33] M. Akbari, A. S. Bahman, P. D. Reigosa, F. Iannuzzo, and M. T. Bina, "Thermal modeling of wire-bonded power modules considering non-uniform temperature and electric current interactions," *Microelectronics Reliability,* vol. 88-90, pp. 1135-1140, 2018.

[34] R. Wu *et al.*, "A Temperature-Dependent Thermal Model of IGBT Modules Suitable for Circuit-Level Simulations," *IEEE Transactions on Industry Applications,* vol. 52, no. 4, pp. 3306-3314, 2016.

[35] W.-S. Loh, M. Corfield, H. Lu, S. Hogg, T. Tilford, and C. M. Johnson, "Wire Bond Reliability for Power Electronic Modules - Effect of Bonding Temperature," in Proceedings of 2007 International Conference on Thermal, Mechanical and Multi-Physics Simulation Experiments in Microelectronics and Micro-Systems (EuroSime), London, UK, 16-18 April, 2007, pp. 1-6.

IEEE POWER ELECTRONICS REGULAR PAPER/LETTER/CORRESPONDENCE

[36] E. Arjmand, P. A. Agyakwa, M. R. Corfield, J. Li, B. Mouawad, and C. Mark Johnson, "A thermal cycling reliability study of ultrasonically bonded copper wires," *Microelectronics Reliability,* vol. 59, pp. 126-133, 2016.

[37] R. Ruffilli, "Fatigue mechanisms in Al-based metallizations in power MOSFETs," Ph.D. dissertation, École doctorale Sciences de la Matière, Universit éPaul Sabatier (Toulouse 3), 2017.

[38] F. Z. Ralf Schmidt, "Impact of absolute junction temperature on power cycling lifetime," in Proceedings of 15th European Conference on Power Electronics and Applications (ECCE Europe), Lille, France, 2-6 Sept., 2013, pp. 1-10.

[39] P. Paris and F. Erdogan, "A critical analysis of crack propagation laws," *Journal of Basic Engineering,* vol. 84, no. 4, pp. 28-533, 1963.

[40] G. Khatibi, M. Lederer, B. Weiss, T. Licht, J. Bernardi, and H. Danninger, "Accelerated mechanical fatigue testing and lifetime of interconnects in microelectronics," *Procedia Engineering,* vol. 2, no. 1, pp. 511-519, 2010.

[41] H. Tada, P. C. Paris, and G. R. Irwin, *The Stress Analysis of Cracks Handbook*, Third Edition ed. New York: ASME Press, 2000.

[42] N. R. Mohsin, "Comparison Between Theoretical and Numerical Solutions for Center, Single Edge and Double Edge Cracked Finite Plate Subjected to Tension Stress," *International Journal of Mechanical and Production Engineering Research and Development,* vol. 5, no. 2, pp. 11-20, 2015.

[43] Y. Lu and A. Christou, "Prognostics of IGBT modules based on the approach of particle filtering," *Microelectronics Reliability,* vol. 92, pp. 96-105, 2019.

[44] C. Durand, M. Klingler, D. Coutellier, and H. Naceur, "Failure mechanisms and reliability of the Al-chipmetallization during power cycling," in Proceedings of 22 ème Congrès Français de Mécanique, Lyon, France, 24-28 August, 2015, pp. 1-19.

[45] M. Brincker, K. B. Pedersen, P. K. Kristensen, and V. Popok, "Passive thermal cycling of power diodes under controlled atmospheric conditions - effects on metallization degradation," in Proceedings of 9th International Conference on Integrated Power Electronics Systems (CIPS), Nuremberg, Germany, 8-10 March, 2016, pp. 1-6.

[46] Y. Yamada *et al.*, "Reliability of wire-bonding and solder joint for high temperature operation of power semiconductor device," *Microelectronics Reliability,* vol. 47, no. 12, pp. 2147-2151, 2007.

[47] A. Fulop and J. Li, "Efficient learning via simulation: A marginalized resample-move approach," *Journal of Econometrics,* vol. 176, no. 2, pp. 146-161, 2013.

[48] S. Hartmann and E. Özkol, "Bond wire life time model based on temperature dependent yield strength," in Proceedings of 2012 International Conference for Power Electronics, Intelligent Motion, Power Quality and Energy Management (PCIM Europe), Nuremberg, Germany, 8-10 May, 2012.